Evidence of parametric instabilities in second harmonic spectra from 1054 nm laser-produced plasmas

K. Tanaka, W. Seka, L. M. Goldman, M. C. Richardson, R. W. Short, J. M. Soures, and E. A. Williams[a)]

Laboratory for Laser Energetics, University of Rochester, 250 East River Road, Rochester, New York 14623

(Received 27 March 1984; accepted 9 May 1984)

Second harmonic spectra emitted from 1054 nm laser-produced plasmas have been observed in side- and backscattering and are shown to have angularly dependent, complex structures. Sidescattered spectra show regularly spaced (~ 20 Å) Stokes components at intensities above 5×10^{13} W/cm^2. The Stokes components are polarized and stronger in the plane of the polarization of the incident laser. These Stokes components are interpreted to be caused by a combination of electron plasma waves generated by the parametric decay instability and the subsequent electron decay instability. Backscattered spectra show additional finely spaced red-shifted satellites above 4×10^{14} W/cm^2, indicative of the electron decay instability of plasmons generated from resonance absorption.

I. INTRODUCTION

Reported here are spectroscopic studies of second harmonic (2ω) light emission from plasmas produced by 1054 nm irradiation of spherical and planar targets. Earlier studies[1-5] on this subject have shown that the 2ω emission results from both linear and nonlinear laser-plasma interaction mechanisms near the critical density (n_c). Mainly two interaction processes contribute to 2ω emission: resonance absorption, which involves linear conversion of incident photons into electron-plasma (ep) waves at n_c, and the parametric decay instability (PDI), in which the incident electromagnetic (em) wave decays into an ep wave and ion-acoustic (ia) wave just below n_c. The second harmonic light with frequency $2\omega_L$, where ω_L is the pump laser frequency, can be generated by scattering incident photons off resonance absorption plasmons. A combination of two PDI plasmons can create the 2ω light, whose frequency is red-shifted by twice the ion acoustic frequency. Spectroscopic analysis of the 2ω light can thus provide information about laser-plasma interactions occurring near the critical density. The importance of studying these interaction mechanisms lies in the potential of the generated plasma waves to produce energetic electrons. In case of spherical targets irradiated with 24 laser beams, we observe a primary peak at $2\omega_L$ and as many as four well-defined down-shifted Stokes components evenly spaced with successively decreasing intensity. For planar target experiments, measurements of the angular distribution and the polarization dependence of the 2ω spectra have been made along with measurements of the signal intensity in and out of the plane of the polarization of the incident laser. Sidescattering spectra observed at 45° for planar targets irradiated at normal incidence are essentially identical to those observed in spherical illumination. The Stokes components of these spectra are polarized and stronger in the plane of the polarization than out. In contrast, the backscattered spectra at intensities above 4×10^{14} W/cm^2 show many closely spaced red-shifted peaks, whereas much weaker Stokes components are seen at the lower laser intensities with spacings similar to those observed in sidescattering.

II. EXPERIMENTAL ARRANGEMENT

The experiments were conducted on both the 24 beam OMEGA laser[6] ($\lambda_L = 1054$ nm, $\tau_L = 1$ nsec, $E_L \leqslant 2$ kJ, $I_L \leqslant 5\times 10^{14}$ W/cm^2) and the single beam GDL laser system[7] ($\lambda_L = 1054$ nm, $\tau_L = 1$ nsec, $E_L \leqslant 60$ J, $I_L \leqslant 10^{15}$ W/cm^2) at the Laboratory for Laser Energetics. Targets were CH, Cu, or Ta coated CH spheres and glass microballoons (200–400 μm diameter) for the 24 beam irradiation, and mostly planar 100 μm thick CH foils for the single beam experiments. For spherical geometry, the laser was focused through $f/4$ lenses tangentially onto the targets with overlapping beams. An $f/12$ lens was used for planar targets and produced a 100 μm spot. Using a grating spectrograph, the 2ω spectra were measured with a dynamic range of over three orders of magnitude with a spectral resolution $\Delta\lambda \leqslant 2$ Å. In the 24 beam experiments the sidescattered spectra were observed between incident beams at about 22.5° with respect to the nearest beam. In the planar target experiments, both backscattering through the focusing lens and the sidescattering at 45° in the horizontal plane were measured, using either horizontal or vertical polarization of the incident laser.

III. EXPERIMENTAL RESULTS

Figure 1 shows typical 2ω spectra obtained from a spherical CH plasma with 24 beam illumination. The spectra for three different intensities are normalized to the primary peak intensity. At the lowest laser intensity, such as seen in Fig. 1(a), three distinct peaks are seen. The primary peak is traditionally identified as scattering of incident photons off

[a)] Present address: Lawrence Livermore National Laboratory, Livermore, California 94550.

 0031-9171/84/082187-04$01.90

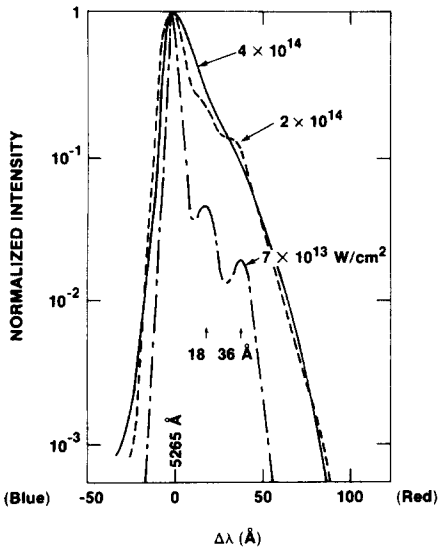

FIG. 1. Normalized 2ω spectra from spherical CH plasma with 24 beam illumination.

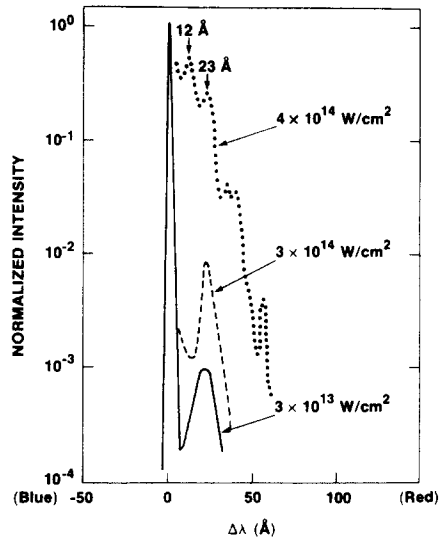

FIG. 3. 2ω backscatter spectra from planar CH plasma.

ep waves generated by resonance absorption.[2,3] Two Stokes peaks are located at 18 and 36 Å to the red of the primary peak. These spectral locations have been found to be independent of irradiation intensity (Fig. 1), as well as target material. Furthermore these peaks are only observed above $I_L \cong 5\times 10^{13}$ W/cm^2. This type of Stokes component was observed in Refs. 3 and 5 and was attributed to a combination of plasmons from the PDI. As seen in Figs. 1(b) and 1(c), at higher intensities the peaks merge into a continuum on the red side of the primary peak. More detailed discussions of these Stokes components will follow below.

In Fig. 2 we show the intensity scaling of the energy in the primary peak and the first Stokes peak relative to the incident energy. As evident from the figure, the Stokes component grows much faster with laser intensity than the primary peak, indicating the existence of nonlinear coupling for this Stokes component. The primary peak follows an intensity dependence of $E_{2\omega}/E_\omega \propto I_L^{1.5}$, where $E_{2\omega}$, E_ω are the energy in the 2ω primary peak and laser. The observed scaling is somewhat stronger than the expected linear scaling. This may be caused by the intensity dependence of inverse bremsstrahlung (IB) absorption: as the incident intensity increases, IB absorption decreases, causing more of the incident light to reach the critical density. Since resonance absorption depends on the light reaching critical the flux of ep waves may be expected to scale faster than linearly, consistent with Fig. 2.

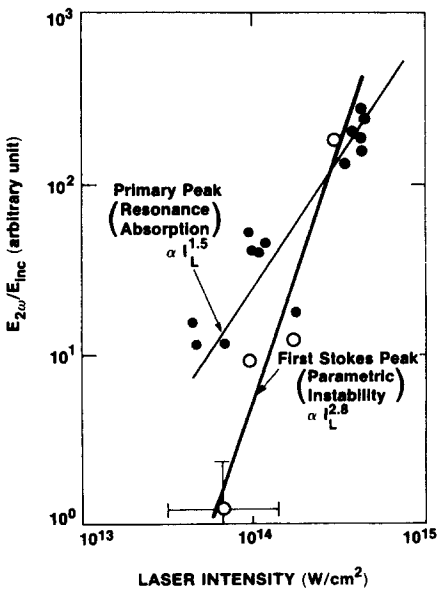

FIG. 2. Energy in the primary 2ω peak (●) and the first Stokes peak (○) relative to the incident energy as a function of irradiation intensity. (Solid lines are fits to the data.)

In the single beam experiments, we have investigated the angular dependence of the 2ω spectra, the dependence of the sidescattered spectra on the incident polarization, and the degree of polarization of the various types of 2ω spectra.

The sidescattered spectra obtained for planar geometry are very similar to the ones from the spherical geometry, showing two to three distinct Stokes peaks in addition to the primary peak at the lower intensities. If the primary peak originates from resonance absorption, this should be specularly reflected and should have the same polarization as the incident laser. The observation at a specular angle of 45° (target at 22.5° to the laser axis) shows, in fact, that the primary peak intensity increases by an order of magnitude compared to normal incidence, and is highly polarized (10:1).

The Stokes peak in the spectra should also be polarized and should be stronger in the plane of the polarization of the incident em wave, provided that this red-shifted peak is a result of the combination of two ep waves from the PDI.[1,2] The measurements for normal incidence of the laser show that the Stokes peaks are polarized (8:1) and that they are three times stronger in the plane of the polarization than out of the plane.

The backscattering spectra from planar CH targets at three different intensities are shown in Fig. 3. At less than 3×10^{14} W/cm^2 [Figs. 3(a) and 3(b)] the spectra resemble the sidescatter spectra in Fig. 1. The shift of the Stokes compo-

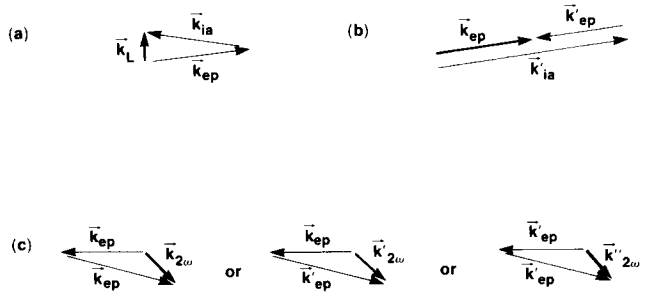

FIG. 4. Scattering diagrams of parametric decay instability (a), electron decay instability (b), and 2ω generation using combination of photons and plasmons. Plasmon wave vectors are denoted by k_{ep}, photon wave vectors by k_L (incident laser) and $k_{2\omega}$ (scattered 2ω light), and ion-acoustic wave vectors by k_{ia}. Frequencies associated with $k_{2\omega}$, $k'_{2\omega}$, $k''_{2\omega}$, etc., differ by multiples of $2\omega_{ia}$.

nent is approximately 23 Å (20 Å in the case of the sidescatter), indicating that the same mechanism is likely to be responsible for this spectrum. However, a slight increase of the laser intensity brings up the intensities of the red-shifted peaks to a level comparable to the primary peak, and a number of narrowly spaced red-shifted peaks become apparent. We also note that the first one of the red-shifted peaks lies at 12 Å, almost half the spectral shift observed in sidescattering or in backscattering at the lower intensities. A possible mechanism for the generation of the narrowly spaced peaks is discussed in the following section.

IV. DISCUSSIONS

As mentioned earlier, the Stokes components attributed to the PDI have an observed threshold $I_L = 5\times10^{13}$ W/cm^2. The theoretical threshold for the PDI[8] may be written as

$$I_{\rm th}^{\rm PDI} = 3\times10^{11}\,(T_{\rm eV}/\lambda_\mu^{\,2}L_\mu)\ {\rm W/cm^2}, \tag{1}$$

where $T_{\rm eV}$ is the electron temperature in eV, λ_μ the pump wavelength in μm, and L_μ the density scale length in μm.

For typical values of these parameters, $T_e = 1$ keV, $L_\mu = 15\,\mu$m, provided from 2-D hydrodynamic code simulations,[9] the theoretical estimate becomes $I_{\rm th}^{\rm PDI} = 2\times10^{13}$ W/cm^2. The difference between this and the observed threshold may be attributed to IB absorption which reduces the effective pump intensity available for the PDI from the nominal intensity.

We now examine the Stokes components in the sidescattering spectra, using the vector diagrams shown in Fig. 4. The k's and ω's refer to the wave vectors and frequencies of the electromagnetic (L), ion-acoustic (ia), and electron-plasma (ep) waves, respectively. These figures indicate approximate k-matching conditions. Here the density gradient is taken parallel to the incoming laser wave vector.

For the first Stokes component, the two mechanisms shown in Figs. 4(a) and 4(c) are involved. The PDI produces plasmons almost perpendicular to the incident laser k vector [Fig. 4(a)]. Two plasmons, each of frequency $\omega_{ep} = \omega_L - \omega_{ia}$, are combined to generate the 2ω light with a frequency shift $\Delta\omega = 2\omega_{ia}$. Since this generation mechanism can be viewed as the inverse of the two-plasmon decay instability with large $k_\perp$ (component of k perpendicular to ∇n), the emission should peak near 45° with respect to the incident laser axis as shown in Fig. 4(c).[10] This is consistent with the observation that the Stokes components are considerably weaker in backscattering than in sidescattering. In contrast to the interpretation in Ref. 5, a combination of PDI plasmons and incident photons is not likely to generate a Stokes component because the k-matching condition cannot be satisfied.

From energy and momentum conservation and the dispersion relations, the frequency or wavelength shift for the first Stokes component may be expressed as

$$\frac{\Delta\omega}{\Delta\omega_{2\omega}} = \frac{\Delta\lambda}{\lambda_{2\omega}} = \frac{1}{\sqrt{3}}\frac{c_s}{v_e}\left(1-\frac{n_e}{n_c}\right)^{1/2}, \tag{2}$$

where c_s and v_e are the ion-acoustic and the electron thermal speeds, n_e is the electron density at which the PDI occurs and where the 2ω light is generated. Substituting the observed wavelength shift of 20 Å into Eq. (2), we obtain $n_e = 0.83\,n_c$. Evaluating the Debye length ($\lambda_{\rm D}$) at this density for a temperature $T_e = 1$ keV, we find $k_{ep}\lambda_{\rm D} = 0.25$, which is in agreement with the simulation results for the most unstable wave seen in Ref. 11.

The second satellite peak in the sidescatter spectra shows exactly twice the shift of the first peak. To interpret this, another decay process is needed as shown in Fig. 4(b). Here an ep wave (k_{ep}) from the primary PDI decays into a secondary ep wave (k'_{ep}) and an ia wave (k'_{ia}) via the electron decay instability (EDI).[12] The threshold for the EDI is expected to be very low because of the long effective scale length normal to the density gradient. The theoretical threshold may be given as

$$I_{\rm th}^{\rm EDI} = 4\times10^{6}\,(T_{\rm eV}^2/L_\mu\lambda_\mu)\ {\rm W/cm^2}. \tag{3}$$

With $T_e = 1$ keV and $L_\mu = 80\,\mu$m (we take the lateral density scale length to be half of the target radius), we find $I_{\rm th}^{\rm EDI} = 5\times10^{10}$ W/cm^5. Thus the second satellite peak in sidescattering can be produced with a very small fraction ($<0.1\%$) of the incident energy converted into the plasmons via the PDI. Electron plasma waves generated by EDI have a frequency shift with respect to ω_L of $\Delta\omega = \omega_{ia} + \omega'_{ia} = 3\omega_{ia}$, since $\omega'_{ia} = k'_{ia}c_s = 2k_{ep}c_s = 2\omega_{ia}$. Thus the combination of two ep waves from the EDI and the PDI can give rise to further Stokes peaks with frequency shifts equal to multiples of $2\omega_{ia}$ as shown in Fig. 4(c) and referred to as $k'_{2\omega}$ and $k''_{2\omega}$.

The backscattering spectra in Fig. 3 show a number of finely spaced, red-shifted peaks at $I_L \cong 4\times10^{14}$ W/cm^2, very different from the spectra obtained in sidescattering. We propose that these peaks originate from the EDI of the ep waves from resonance absorption traveling down the density gradient. In contrast to the EDI associated with the PDI we expect a higher threshold for this instability because of the shorter scale length applicable here. Refraction causes plasmons to be directed along the density gradient. Thus the relevant density scale length is given by the density gradient near n_c. This explains why we do not observe the narrowly spaced backscattering peaks below 4×10^{14} W/cm^2. Substi-

tuting the observed wavelength shift of 12 Å into Eq. (2), we obtain $n_e = 0.96\, n_c$. This indicates that the 2ω satellites observed in the backscattering are generated much closer to the critical density than those obtained in the sidescattering.

V. CONCLUSION

Our measurements have revealed significant details of the 2ω spectra emitted from both spherical and planar plasmas. The sidescattered 2ω spectra, as well as spectra from spherically irradiated plasmas, show a primary peak at $2\omega_L$ and several Stokes lines separated by approximately 20 Å. We identify the primary peak as caused by resonance absorption. The first Stokes peak originates from the combination of two ep waves from the PDI. The second and subsequent Stokes lines are caused by the combination of the ep waves from the PDI and secondary plasmons produced by the EDI. The results are consistent with PDI plasmons generated with wave vectors near the Landau damping limit ($k\lambda_D = 0.25$). The backscattering spectra are similar to, but weaker than, the sidescatter spectra at intensities below 3×10^{14} W/cm^2. At higher intensities the backscattering spectra show many narrowly spaced red-shifted peaks. We interpret these peaks as resulting from scattering of incident photons off secondary ep waves generated by the decay via EDI of resonance absorption plasmons propagating down the density gradient.

ACKNOWLEDGMENTS

We are grateful to Dr. R. S. Craxton for many valuable suggestions. This work was supported by the U.S. Department of Energy Inertial Fusion Project under Contract No. DE-AC08-80DP40124 and by the Laser Fusion Feasibility Project at the Laboratory for Laser Energetics which has the following sponsors: General Electric Company, Northeast Utilities Service Company, Southern California Edison Company, New York State Energy Research and Development Authority, The Standard Oil Company (Ohio), The University of Rochester, and Empire State Electric Energy Research Corporation. Such support does not imply endorsement of the content by any of the above parties.

[1] C. Yamanaka, T. Yamanaka, T. Sasaki, J. Mizui, and H. B. Kang, Phys. Rev. Lett. **32**, 1038 (1974).
[2] R. Sigel, J. Phys. (Paris) **38**, c6–35 (1977).
[3] N. G. Basov, V. Yu. Bychenkov, O. N. Krokhin, M. V. Osipov, A. A. Lupasov, V. P. Silin, and G. V. Sklizkov, Sov. Phys. JETP **49**, 1059 (1979).
[4] S. Jackel, S. Eliezer, and A. Ziegler, Phys. Rev. A **24**, 1601 (1981).
[5] X. Zhizhan, X. Yuguang, Y. Guangyu, Z. Yanzhen, Y. Jiajin, and P. H. Lee, J. Appl. Phys. **54**, 4902 (1983).
[6] J. Bunkenberg, J. Boles, D. C. Brown, J. Eastman, J. Hoose, R. Hopkins, L. Iwan, S. D. Jacobs, J. H. Kelly, S. Kumpan, S. Letzring, D. Lonobile, L. Lund, G. Mourou, S. Refermat, W. Seka, J. M. Soures, and K. Walsh, IEEE J. Quantum Electron. **QE-17**, 1620 (1981).
[7] W. Seka, J. Soures, O. Lewis, J. Bunkenberg, D. Brown, G. Mourou, and J. Zimmerman, Appl. Opt. **19**, 409 (1980).
[8] F. W. Perkins and J. Flick, Phys. Fluids **14**, 2012 (1971).
[9] R. S. Craxton, computer code SAGE (Laboratory for Laser Energetics, University of Rochester, New York, 1984).
[10] A. Simon, R. W. Short, E. A. Williams, and T. Dewandre, Phys. Fluids **26**, 3107 (1983).
[11] Laser Program Annual Report, 1981, Lawrence Livermore National Laboratory, Livermore, CA, UCRL-50021-81, pp. 3–40.
[12] F. F. Chen, *Introduction to Plasma Physics* (Plenum, New York, 1974), p. 259.